Elsevier Editorial System(tm) for Materials and Design

Manuscript Draft

Manuscript Number: JMAD-D-18-02281R1

Title: Ternary composite solid-state flexible supercapacitor based on nanocarbons/manganese dioxide/PEDOT:PSS fibres

Article Type: Research Paper

Keywords: fibre supercapacitor; carbon nanotube; wet-spinning; manganese oxides; PEDOT:PSS; energy storage

Corresponding Author: Dr. Jose Garcia-Torres, Ph.D.

Corresponding Author's Institution: Technical University of Catalonia

First Author: Garcia Jose, Ph.D.

Order of Authors: Garcia Jose, Ph.D.; Carol Crean

Abstract: Flexible fibre supercapacitors were fabricated by wet-spinning from carbon nanotube/carbon black dispersions, followed by straightforward surface treatments to sequentially deposit MnO2 and PEDOT:PSS to make ternary composite fibres. Dip coating the fibres after the initial wet-spinning coagulation creates a simple solution-based continuous process to produce fibre-based energy storage. Well-controlled depositions were achieved and have been optimised at each stage to yield the highest specific capacitance. A single ternary composite fibre exhibited a specific capacitance of 351 F g-1. Two ternary composite fibre electrodes were assembled together in a parallel solid-state device, with polyvinyl alcohol/H3PO4 gel used as both an electrolyte and a separator. The assembled flexible device exhibited a high specific capacitance of 51.3 F g-1 with excellent both charge-discharge cycling (84.2% capacitance retention after 1000 cycles) and deformation cycling stability (82.1% capacitance retention after 1000 bending cycles).

*Graphical Abstract
Click here to download high resolution image

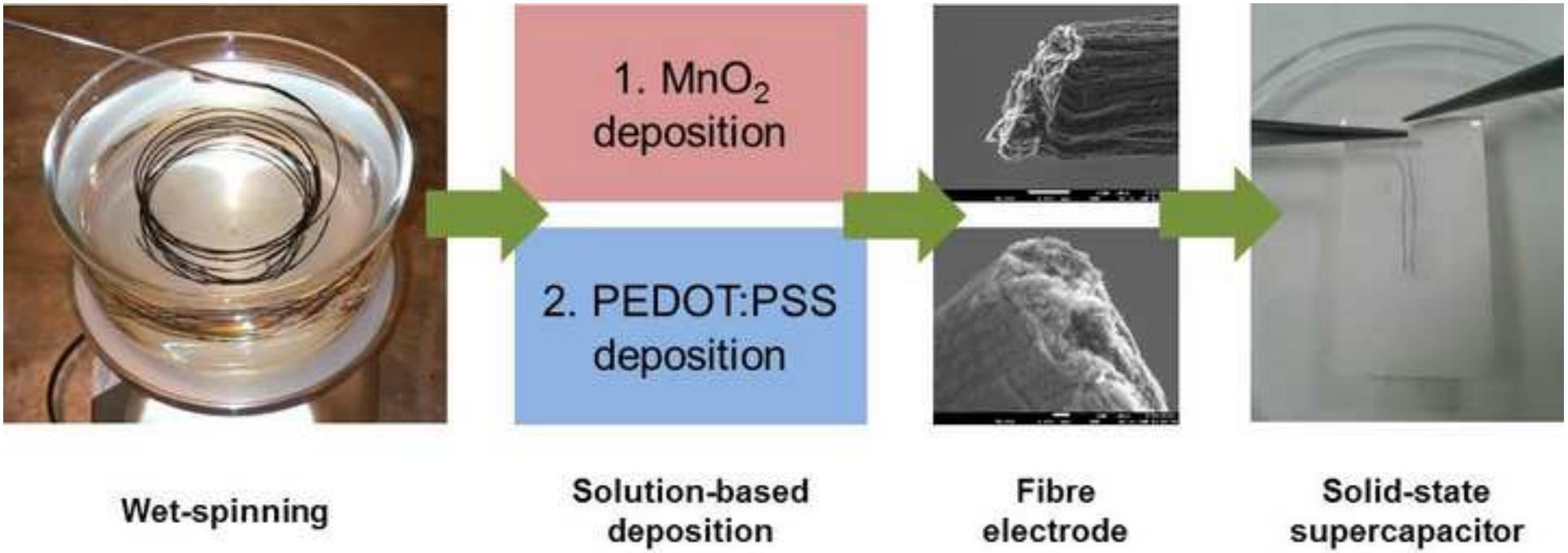

Highlights

- Carbon-MnO_2-PEDOT:PSS composite fibres have been prepared by all aqueous solution based depositions.
- Ternary composite fibres show fexibility and excellent energy storage capacity.
- Ternary fibres can be assembled in solid-state supercapacitors with good capacitive performance and promising applicability in wearable electronics.

Ternary composite solid-state flexible supercapacitor based on nanocarbons/manganese dioxide/PEDOT:PSS fibres

José Garcia-Torres[a,1,*] and Carol Crean[a]

[a] Department of Chemistry, University of Surrey, Guildford, Surrey, GU2 7XH, UK

*Corresponding author: Dr. Jose Garcia-Torres: Tel.: (+34) 93 413 73 29. E-mail: jose.manuel.garcia-torres@upc.edu

GRAPHICAL ABSTRACT

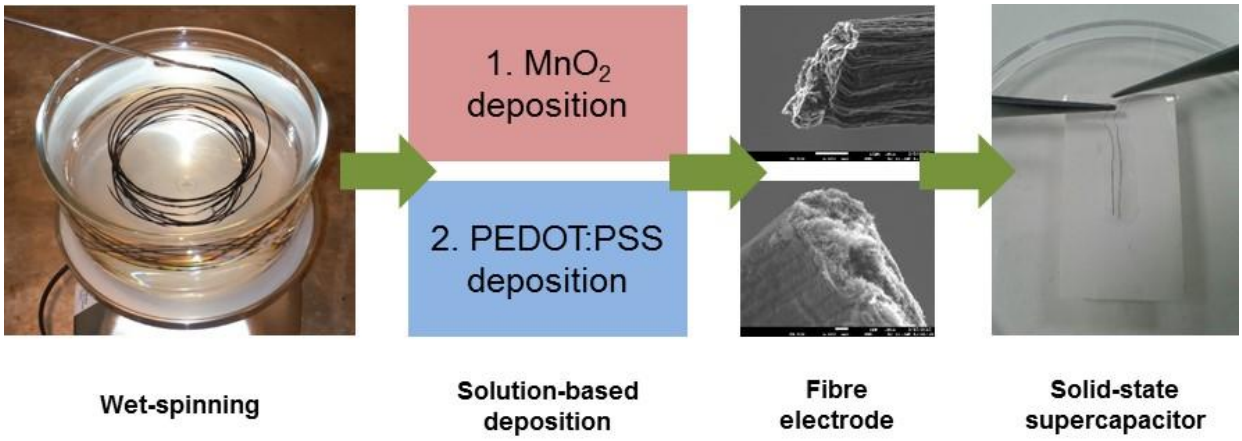

[1] Present Address: Serra Húnter Fellow at Department of Materials Science and Metallurgical Engineering, Universitat Politècnica de Catalunya, Av. Eduard Maristany, 10-14, 08019, Barcelona, Spain.

ABSTRACT

Flexible fibre supercapacitors were fabricated by wet-spinning from carbon nanotube/carbon black dispersions, followed by straightforward surface treatments to sequentially deposit MnO_2 and PEDOT:PSS to make ternary composite fibres. Dip coating the fibres after the initial wet-spinning coagulation creates a simple solution-based continuous process to produce fibre-based energy storage. Well-controlled depositions were achieved and have been optimised at each stage to yield the highest specific capacitance. A single ternary composite fibre exhibited a specific capacitance of 351 F g^{-1}. Two ternary composite fibre electrodes were assembled together in a parallel solid-state device, with polyvinyl alcohol/H_3PO_4 gel used as both an electrolyte and a separator. The assembled flexible device exhibited a high specific capacitance of 51.3 F g^{-1} with excellent both charge-discharge cycling (84.2% capacitance retention after 1000 cycles) and deformation cycling stability (82.1% capacitance retention after 1000 bending cycles).

Keywords: fibre supercapacitor, carbon nanotube, wet-spinning, manganese oxides, PEDOT:PSS, energy storage

1. INTRODUCTION

Wearable electronic devices have attracted much attention in recent years because of their widespread applicability from personal electronics, to healthcare applications such as sensors, actuators, transistors, fuel cells and solar cells [1,2]. To be truly wearable, lightweight and flexible energy storage is essential to power such electronics. Fibre-shaped electrodes are emerging as a versatile design for wearable applications since they can be easily incorporated into clothing [3]. Applications of fibre-based electrodes in the storage of energy include examples of battery [4] and supercapacitor devices [5]. Among them, supercapacitors were deemed as the most promising devices for wearable electronics due to the long cycling life, high power density, fast charge-discharge capability and safe operation [6].

Studies on fibre-based supercapacitors have mainly focused on the development of novel electrode materials that can be formed as a fibre as they have a critical impact on the electrochemical performance of the supercapacitor [7,8]. Carbon nanomaterials (typically, carbon nanotubes (CNT) or graphene) have many properties that make them suitable for wearable electrodes including being lightweight and possessing high mechanical strength together with good electrical conductivity that permits fast charge transport. However, they show some drawbacks that limit their applicability like low capacitance values, slow production rates or high cost [6,9]. For such reasons, recent progress in fibre-based supercapacitors has focused on the fabrication of multi-component composite fibres due to their enhanced properties. Thus, carbon-carbon composite fibres have shown improved energy storage properties over their single component counterparts. The introduction of other nanostructured carbons (ordered mesoporous carbons, graphenes) into CNT fibres combines the advantages of both materials [10]. Examples of fibres made from different carbons include a reduced graphene oxide (rGO)/CNT fibre [11], hybrid CNT/ ordered mesoporous

carbon fibre [10] and CNT/graphene yarn [12] to mention but a few. On the other hand, combining pseudocapacitive materials such as transition metal oxides or conducting polymers with nanostructured carbons results in excellent supercapacitors due to the synergistic effects of increased electrical conductivity and specific capacitance [13]. Among metal oxides, the natural abundance of MnO_2 renders it a highly sustainable resource for next generation energy storage devices. In many cases, the metal oxide and conducting polymer are electrochemically deposited onto the carbon-based fibre [13]. Normally, these pseudocapacitive materials are grown in the fibre surface layer, forming a core-shell structure, and the core does not participate in loading. In this circumstance, the core carbon fibre just acts as a fibre scaffold and current collector while the pseudocapacitive shell contributes to the majority of energy storage. For exemple, Choi *et al.* developed a CNT fibre coated with flower-shaped MnO_2 nanoparticles [14]. The MnO_2 shell layer was 200–300 nm thick and the weight percentage of MnO_2 was 4.44–6% of total mass. Although the fraction of MnO_2 was low, the area of cyclic voltammetry curve was approximately 5 folds of that before deposition. Similarly, Shang *et al.* coated CNT fibres with polypyrrole (PPy) (PPy total weigth:12.5 wt%) showing a capacitance 5.4 times higher than the original value [15]. The drawback of such strategy is that increasing the thickness of active materials reduces the accessible surface area of the pseudocapacitive materials. Therefore, the incorporation of active materials into the fibre represents a real alternative as the ion and electron transportations are facilitated. Flexible fibres with higher psuedocapacitive material contents and excellent capacitance values are obtained [16-19]. However while such a combination of materials and strategy can yield excellent charge storage capabilities, the steps involved in fibre formation are complex and not easily scalable.

For this reason, the second point of interest is the selection of an appropriate technique not only to improve fibre structure by increasing the specific surface area but also with potential scalability for practical engineering applications. Wet-spinning is a very suitable approach for the macroscale assembly of carbon nanomaterials into continuous and large-scale fibres [20,21]. In this work, we are combining two different carbon nanomaterials –carbon black and CNT- to prepare the fibres for various reasons: (i) the possible synergistic effect between both nanomaterials resulting in an improvement of the electrochemical, electrical, etc properties of the fibre, (ii) the possibility to have a more open structure in the fibre because of the different aspect ratio of the nanomaterials (spheres and tubes) and (iii) the reduction of total cost of the supercapacitor device because the lesser cost of carbon black. On the other hand, post-spinning solution deposition processes can be easily combined with the wet spinning process to get multimaterial fibres with better energy storage performance. Consequently, there is still challenging for the development of high-performance wet-spun multimaterial fibre-based supercapacitors.

Here we present a process involving wet-spinning of CNT-carbon black fibres, which were chemically coated with MnO_2 followed by dip-coating with PEDOT:PSS (poly(3,4-ethylenedioxythiophene)-poly(styrenesulfonte) to create a ternary composite fibre-based supercapacitor with high specific capacitances. Carbon back was wet-spun together with CNTs with a view to improve the electrochemical and electrical properties of the fibre and also reduce the total cost of the supercapacitor. After that, manganese dioxide was first introduced into the fibres by chemical reduction of $KMnO_4$ in order to improve capacitance. The resulting fibres were dip-coated with PEDOT:PSS to improve capacitance and electrical conductivity of the fibres. Finally, two ternary composite fibre electrodes were assembled together in a parallel solid-state supercapacitor, with polyvinyl alcohol/H_3PO_4 gel used as

both an electrolyte and a separator. The resulting device showed good capacitance values and cycle life with little change observed after multiple bendings.

2. EXPERIMENTAL

2.1 Chemicals

Carbon black and carbon nanotubes were purchased from Timcal Graphite & Carbon and Nanocyl, respectively. Chitosan powder, acetic acid (99.8%), sodium dodecyl benzene sulfonate (SDBS), phosphate buffered saline (PBS), polyvinyl alcohol (PVA), phosphoric acid and PEDOT:PSS pellets were obtained from Sigma Aldrich. Potassium permanganate ($KMnO_4$) was obtained from Acros Organics and ethanol from Fisher Chemicals.

2.2 Preparation of fibres

Carbon nanomaterial-based fibres were prepared by wet spinning. Briefly, wet spinning involves the dispersion of the different carbon nanomaterials in a fluid, extruded out of a spinneret into a coagulation bath that causes the fibre to precipitate, and then solidifies as it emerges. The dispersions were prepared by mixing different amounts of carbon black and carbon nanotubes, but the total concentration was always kept constant at 0.1 wt.%. The concentration of the dispersant was also kept constant at 0.15 wt.%. The dispersions were sonicated in a horn sonicator for 30 min. The amplitude, power and frequency were 30 %, 500 W and 20 kHz, respectively. During sonication, the dispersion was immersed in a water/ice bath in order to avoid overheating. The wet-spinning parameters were as follows: 10 ml/min for dispersion injection into the coagulation bath (0.25 wt.% chitosan + 0.5 wt.% acetic acid solution). The coagulation bath was rotated at 50 rpm.

In a second step, fibres were modified by chemical reduction of $KMnO_4$ with ethanol. Firstly, fibres were immersed into ethanol solution followed by the addition of 0.1 M $KMnO_4$ solution for different times ranging from 5 min to 90 min. Fibres were rinsed in deionised water to remove the excess of $KMnO_4$. Finally, fibres were dip coated into a 0.1 wt.% PEDOT:PSS solution for varying times (from 10 sec to 5 min).

Quasi-solid-state supercapacitors were prepared by placing two ternary composite fibres (5 cm long) parallel to each other and coating 4 cm with a gel electrolyte (PVA-H_3PO_4 1:10), which was dried at room temperature. For electrochemical testing, this device was connected at the electrolyte-free ends and characterised by cyclic voltammetry and galvanostatic charge discharge cycling in both straight and bent positions. The fabricated device is quasi-solid-state since it contains a gel polymer electrolyte, however in this manuscript we will omit the term *quasi* for simplification in agreement with many other authors.

2.3 Characterisation

Electrochemical measurements were performed using the following potentiostats: Gamry Reference 600 and eDAQ EA163 with e-corder 410. A conventional three-electrode cell was used, consisting of the spun fibres as working electrode, a 3 mol dm^{-3} Ag/AgCl reference electrode and a platinum mesh counter electrode. The electrolytes employed were 0.01 mol dm^{-3} PBS solution and 0.1 - 0.5 mol dm^{-3} KCl solution for cyclic voltammetry and cyclic charge-discharge (CCD) experiments respectively. In cyclic voltammetry experiments, fibres were scanned from 0 to 0.8 V with various scan rates (10-100 mVs^{-1}). For GCD, currents densities were in the range 0.1-10 A g^{-1}. The gravimetric capacitance of the fibres was calculated from the galvanostatic discharge curve by Eq. (1):

$$C = \frac{I\ t_d}{m\ \Delta V} \qquad (1)$$

where I, t_d, m and ΔV are the applied current, the discharge time, the total mass of the fibre (including the non-capacitive materials) and the potential window, respectively. Equation (1) was also used to calculate the capacitance of the solid-state supercapacitor however; m was the total mass of the two fibres. The mass of the fibres was determined using a Sartorius MC5 microbalance. They were weight before and after the incorporation of either MnO_2 or PEDOT:PSS in order to know the amount of the incorporated pseudo-capacitive materials. The content of carbon nanomaterials into the fibre (70%) was determined by thermogravimetric analysis. The fibre active materials were in the range 70-98% depending on the conditions employed.

Fibre morphology was evaluated using a JEOL USA JSM-7100F Analytical Field Emission Scanning Electron Microscope (SEM). Samples were mounted on a stainless steel stub and connected to it with silver paint. The diameters of the fibres, in the 30-35 μm range, were measured during inspection of fibre cross sections by SEM. Raman spectroscopy of fibres was measured using a Renishaw Systems 2000 Raman Microscope. A 514 nm green laser was used and measurements were performed at 50x magnification. Powder X-ray diffraction (XRD) profiles were measured on a PANalytical X'Pert Pro PW3179 diffractometer using CuKα and an X'Celerator detector. X-ray photoelectron spectroscopy (XPS) measurements were performed with a PHI 5600 multitechnique system. The binding energies (BE) of the XPS signals of all species have been corrected by assuming C1s signal at 284.6 eV. Dynamic mechanical analysis was performed using a TA Instruments DMA Q800 equipment. Electrical conductivity was evaluated by the four-probe method, where a constant current was applied and the resultant voltage measured by a Keithley 2001 multimeter. Thermogravimetric analyses (TGA) were performed employing a TA Instruments TGA Q500 equipment from room temperature to 900 ˚C at 10 ˚C/min in air.

3. RESULTS AND DISCUSSION

3.1 Preparation of dispersions and carbon-based fibres

Carbon black (CB), carbon nanotube (CNT) and mixed CB/CNT-based fibres were prepared by wet spinning dispersions of these carbon nanomaterials with sodium dodecyl benzene sulfonate into a coagulation bath. A range of optimisation studies were carried out to determine the best dispersions for fibre spinning. The concentration of nano-carbons in the dispersion was kept constant at 0.1 wt. % and within this the ratio of carbon black to carbon nanotubes was varied as detailed below (see Figure 1). The concentration of the dispersant (SDBS) was optimised by modifying the SDBS/carbon ratio from 0.5 to 2. Finally the pH of the dispersions was modified between values of 1.5 and 4.5, with a pH of 1.5 and a SDBS/carbon ratio of 1.5 giving the best electrochemical properties (data not shown). Figure 1 shows a picture of such a dispersion illustrating how homogenous these dispersions are. During optical imaging, neither macroscopic nor microscopic aggregates were observed in any of the dispersions prepared.

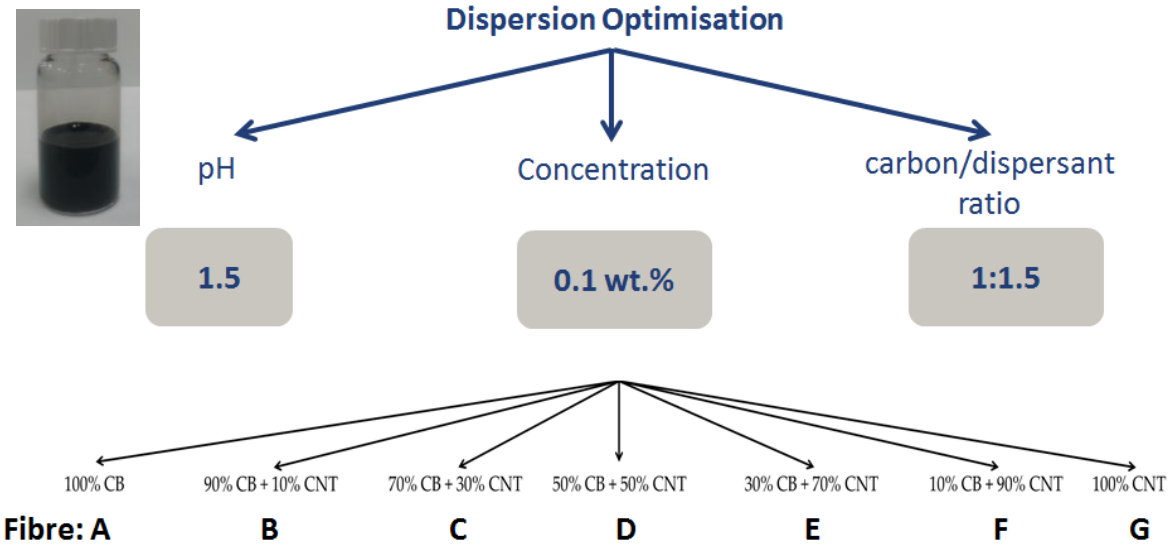

Figure 1. Picture of a dispersion containing 0.05 wt. % CB, 0.05 wt. % CNT, 0.15 wt. % SDBS at a pH of 1.5. Schematic overview of dispersion compositions for optimisation study.

The 7 dispersions detailed in Figure 1 were wet spun into fibres by injection into rotating coagulation baths containing the biopolymer chitosan (Figure 2 top left), which has previously been shown to be an effective coagulant [21]. Fibres were successfully spun from all dispersions and could be made in lengths of metres at a time. Following spinning, the fibres were washed and dried under ambient conditions.

3.2 Fibre structural characterisation

SEM images of fractured cross sections of the fibres made from dispersions of 100% CB, mixed CB:CNT and 100% CNT, are shown in figure 2 (A-G). The fibres containing CNTs clearly show small bundles of CNTs at the cross-sections. The CNTs appear to be aligned parallel to the fibre axis, which may have been induced by the forces on the gel-fibre during the initial stages of coagulation in the rotating coagulation bath.

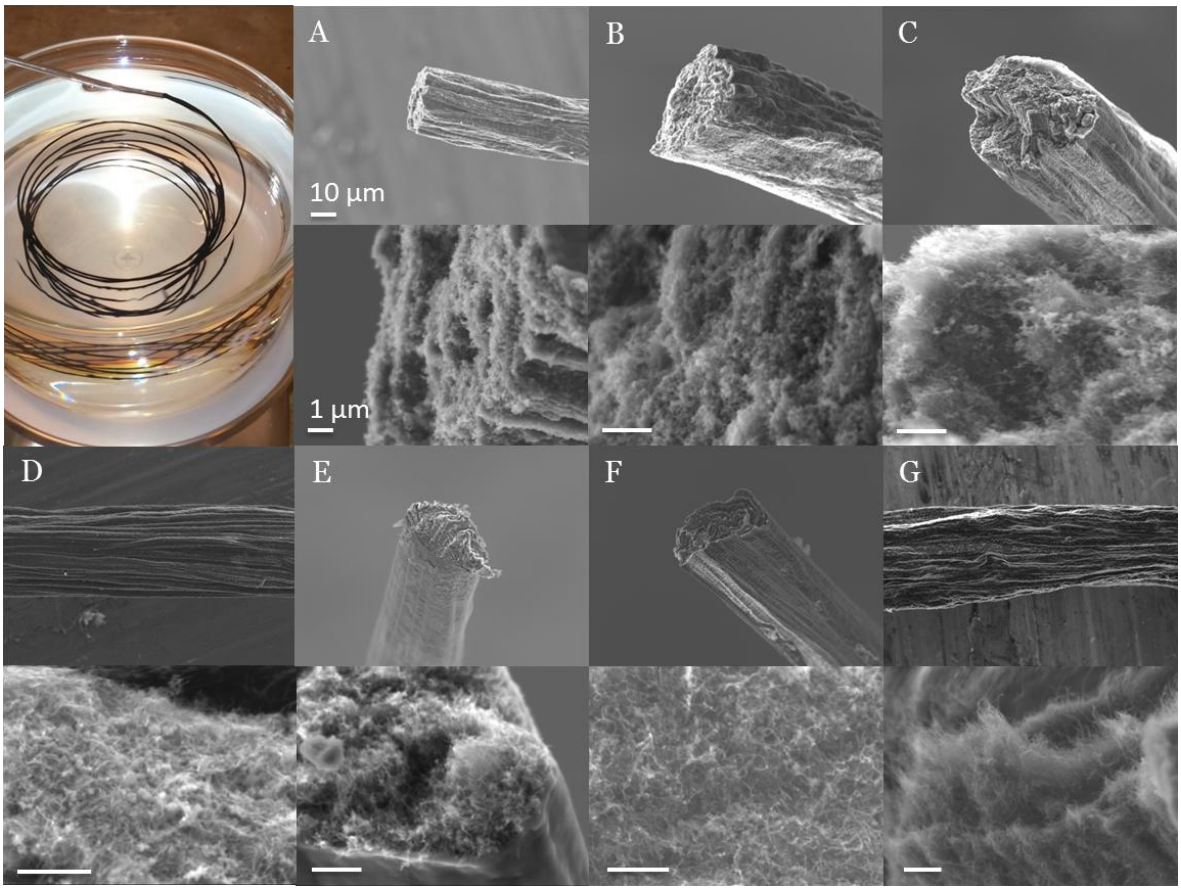

Figure 2. Photograph of wet-spinning of carbon fibres (top left) and SEM images of the surface and cross-sections of fibres containing different amounts of CB and CNT A) 100% CB, B) 90% CB:10% CNT, C) 70% CB:30% CNT, D) 50% CB:50% CNT, E) 30% CB:70% CNT, F) 10% CB:90% CNT, G) 100% CNT.

The fibres appear to have a corrugated surface regardless of their composition. Irrespective of carbon black or nanotube loading, all fibres have an elliptical cross section with diameters of 30-35 µm and appear free of voids. Varying the dispersion composition, from pure CB or pure CNT, to mixtures of CB:CNTs, can clearly be seen by SEM. Close inspection of the fibre cross sections shows an increase in the density of CNT bundles within the fibres as the CNT content of the dispersion is increased, with a corresponding decrease in carbon black

concentration. The fibres appear to be homogeneous across the surface of the cross-section, which suggests that both types of nanomaterials were well dispersed in solution. It also indicates that the CB nanoparticles interact well with CNTs and disperse the CNT bundles. Such well dispersed suspensions have translated into fibres with nanoparticles and nanotubes evenly distributed throughout. Thermogravimetric analyses of these fibres in air indicate that the fibres contain approximately 30 % chitosan regardless of the carbon composition (data not shown).

3.3 Mechanical and electrical properties of fibres

Figure 3 (top) shows the stress-strain curves of these carbon-based fibres, which confirm the reinforcing effect of having both types of nanoparticle within one fibre. CBs and CNTs alone within a chitosan matrix do not interact as favourably as when both particles are together within the fibre. As expected due to the higher aspect ratio, the 100% CNT containing fibres have a higher modulus than the 100% CB-based fibres (11.4 and 6.6 MPa respectively). Both strength and modulus have increased as the composition changed from pure carbon black/carbon nanotube, to mixed composite fibres. 100% CB fibres and 100% CNT fibres have breaking strengths of 8.6 and 13.8 MPa, and breaking strain values of 1.6% and 1.5% respectively. This value increased to 25.2 MPa and 22.9 MPa when composite fibres E (30% CB:70% CNT) and F (10% CB:90% CNT) were measured respectively (with breaking strain values of 4.2% and 2.8% respectively). In addition, modulus values of the composite fibres increased from 11.4 MPa to 18.8 MPa after the addition of 10% CB to the dispersions. These results indicate that there are more favourable interactions between particles within a fibre prepared from a mixed particle (CB:CNT) dispersion, compared to single nanocarbon dispersions.

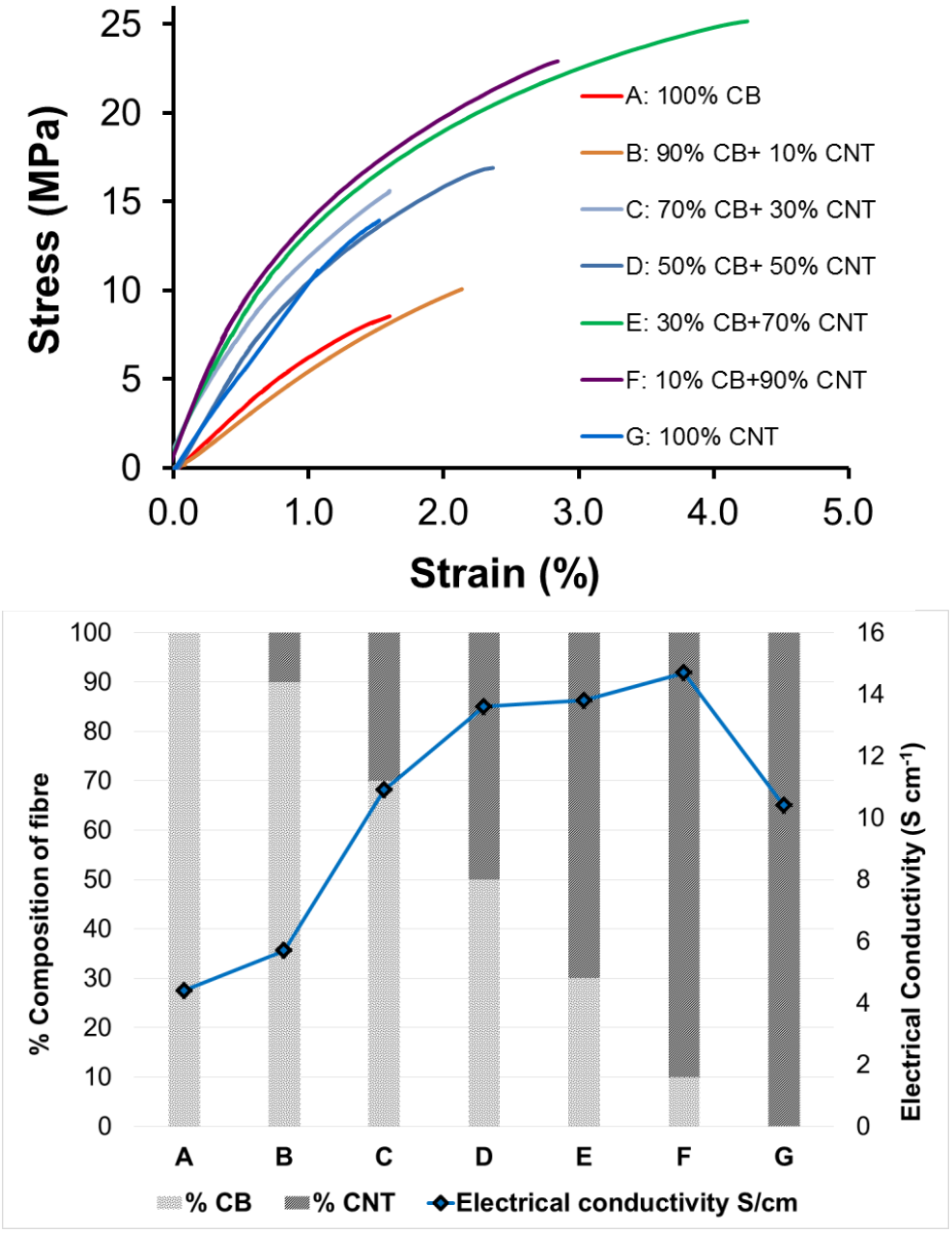

Figure 3. Variation of the mechanical properties (top) and electrical conductivity (bottom) with fibre composition (w.r.t. % CB and CNT).

Spinning dispersions of conducting nanomaterials into the insulating polymer chitosan, produced electrically conducting fibres, the conductivity of which was measured by the four

point probe method. Figure 3 (bottom) illustrates the electrical conductivity of the mixed composite fibres compared to fibres made from either dispersions containing 100% CB or 100% CNT. Increasing the CNT content in CB-containing fibres increased the electrical conductivity from 4.4 S cm^{-1} for Fibre A (100% CB) to 14.7 S cm^{-1} for Fibre F (10% CB:90% CNT). The fibre with the highest conductivity is not Fibre G containing only CNT nanotubes (10.4 S cm^{-1}), but Fibre F made from a dispersion containing 90% CNTs:10% CB, which suggests that carbon black particles act as an effective dispersant for CNTs. Similar synergies have been observed previously for graphene oxide-CNT hybrid materials [22].

Cyclic voltammetry and galvanostatic charge-discharge measurements were carried out in order to determine the capacitance of the composite fibres A-G (Figure S1, S2 and S3). The charge storage mechanism of these fibres is electrochemical double layer capacitance, which is based on the interfacial double-layer of high specific area carbons [22,23]. Substituting part of the CNT content with CB increased the capacitance of these fibres by up to a factor of 2.5, however despite this increase, these capacitance values remain low (12.1 F g^{-1} for Fibre F) in comparison to other carbon-based fibres [5].

3.4 Incorporating pseudocapacitive materials in CB/CNT fibres

Pseudocapacitive materials offer higher specific capacitance than carbons as a result of their redox reactions. Among them, transition metal oxides show the highest capacitance values to date. Manganese oxides were selected as active electrode materials because of their high theoretical specific capacitance of 1370 F g^{-1} [24]. The reversible redox reactions occurring between the MnO_2 on the electrode and the ions in the electrolyte allows Faradaic charge transfer to take place, thereby enhancing the capacitive properties of the fibres. Therefore, in order to improve the capacitive properties of the composite fibres, they were treated with potassium permanganate with a view to reducing the permanganate to an oxide of manganese

on the fibre. This reaction was carried out on Fibre F for times varying between 5 and 60 minutes. Fibre F was chosen because it exhibited the best electrical and electrochemical properties among Fibres A-G.

Figure 4 (A-F) shows SEM images and EDX mapping of the elements carbon and manganese along the surface of Fibre F and cross section following this reaction. It is clear that the fibres treated with potassium permanganate contain manganese in addition to carbon from the nanoparticles of CB, CNT and the polymer chitosan. The XRD pattern of the CB/CNT/MnO_2 composite fibre can be seen in Figure 4G. In addition to the peak corresponding to the CNTs, broad peaks attributed to MnO_2 can be observed at 2θ values of 37°, 42° and 66° [25]. Compared to previously published XRD spectra of MnO_2 this spectrum of the CB/CNT/MnO_2 composite fibre showed very broad peaks which suggests a poorly crystalline manganese dioxide phase in our fibres [26-28].

Raman spectroscopy is useful for analysis of materials exhibiting poor crystallinity. The Raman spectrum of the CB/CNT/MnO_2 composite fibre can be seen in Figure 4H. Two strong peaks measured at 1336 cm^{-1} and 1574 cm^{-1} are associated with the disorder (D-band) and the tangential mode vibrations (G-band) of carbon respectively [29]. Moreover, a sharp peak at 615 cm^{-1} is observed, which is characteristic of the spinel structure of manganese oxides and is attributed to the stretching mode of MnO_6 octahedra [30,31]. Some other weaker peaks are observed in the wavenumber range 300-600 cm^{-1}. Similar peaks have been reported by Adelkhani *et al.* and Han *et al.* and have been assigned to γ-MnO_2 [25,32]. Thus, from RAMAN spectroscopy it seems that no other manganese species (with very characteristic RAMAN spectra like MnOOH) [33] are present. However, fibres were also analysed by X-ray photoelectron spectroscopy (XPS) to corroborate RAMAN findings.

Figure 4I shows that the bending energy separation between the Mn $2p_{1/2}$ and $2p_{3/2}$ doublet peaks is 11.8 eV, in agreement with the reported energy for MnO_2 [34].

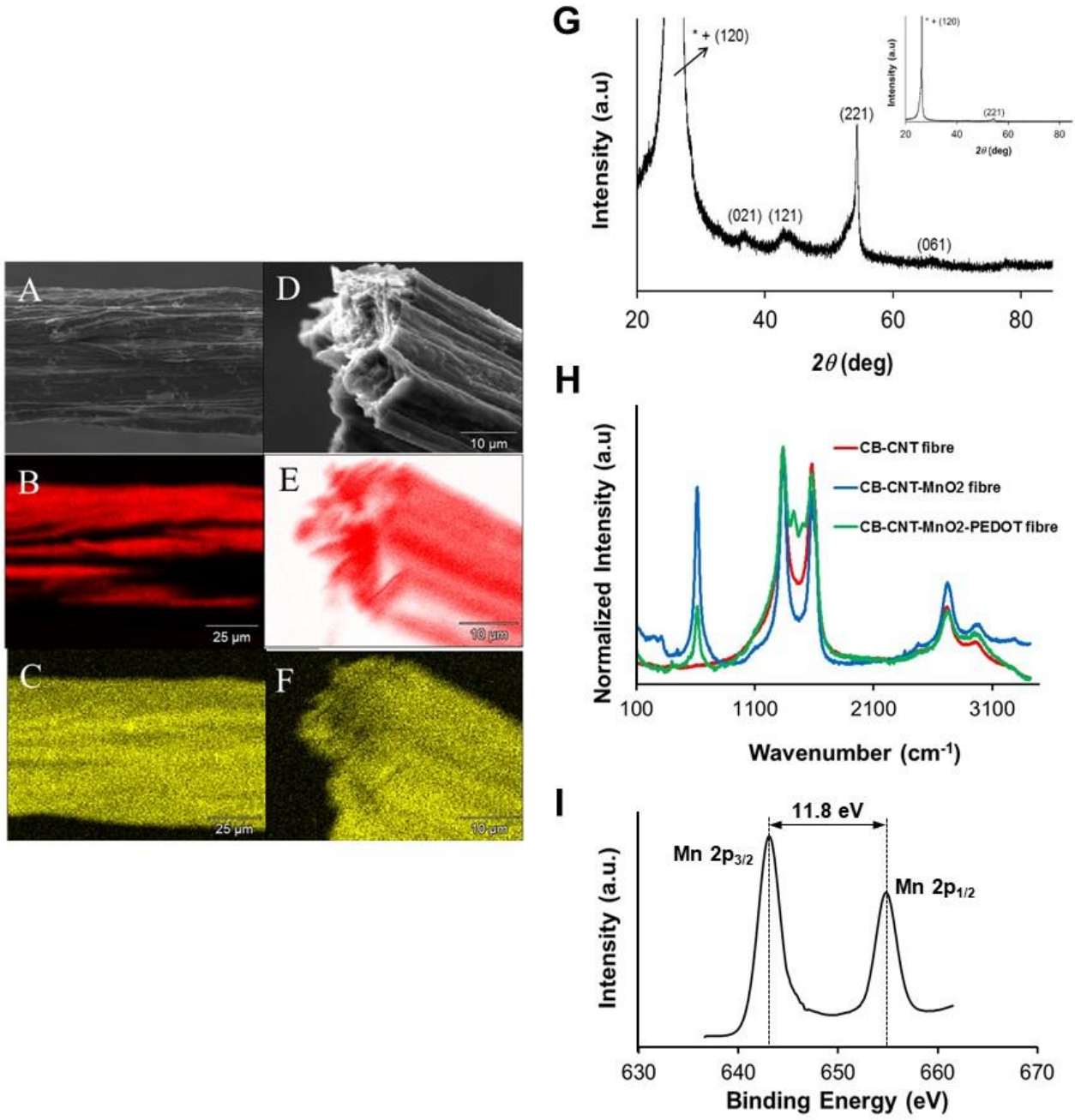

Figure 4. SEM images (A and D) and corresponding EDX maps of fibres following treatment with $KMnO_4$. (B) and (E) show the carbon map, while (C) and (F) show the map of manganese along the fibre surface and cross section respectively. (G) XRD spectrum of the

$KMnO_4$ treated fibre. (H) Raman spectroscopy of carbon-based fibres alone, and following the reduction of $KMnO_4$ on the surface and dip coating with PEDOT:PSS. (I) XPS spectrum of the CB/CNT/MnO_2/PEDOT:PSS fibres.

To evaluate the electrochemical performance of the manganese oxide-containing fibres as supercapacitor electrodes, we first performed galvanostatic charge-discharge measurements in a three-electrode cell (Figure 5A). The results of these experiments indicate that among $KMnO_4$ immersion times of 5, 15, 30, 60 and 120 minutes, the 30 minute treatment proved the most effective in increasing the pseudo-capacitance of the fibres. A capacitance value of approximately 195 F g^{-1} was obtained (applied intensity 0.5 A g^{-1}). This has led to a 16-fold improvement in the capacitive behaviour of the CB/CNT composite fibre (made from a 10% CB-90 % CNT dispersion). The mechanism is based on the reversible surface adsorption/desorption of alkali metal cations ($M^+ = K^+$, Na^+, Li^+) into/from MnO_2:

$$(MnO_2)_{surface} + M^+ + e^- \rightleftharpoons (MnO_2^-M^+)_{surface}$$

with a concomitant redox reaction between the III and IV oxidation states of Mn [35]. Thus, the higher the MnO_2 content, the higher the capacitance. However, if the reduction time exceeds 30 min, a decrease in the capacitance is observed, which can be attributed to a decrease in the electrical conductivity of the fibre because the high electrical resistivity of MnO_2. On the other hand, cyclic voltammetry of CB/CNT/MnO_2 electrodes (Figure 5B) exhibit a nearly rectangular shape within the 10 mV s^{-1} to 100 mV s^{-1} scan rate range, indicating good rate properties (fast ion transportation) as well as excellent electrochemical double layer capacitive characteristics. The good electrical conductivity of the carbon

nanomaterials and the swelling of the chitosan facilitate the electron transport within the fibre and enhance the electrochemical utilization of MnO_2.

However, metal oxide specific capacitance depends on electrical conductivity, morphology, and particle size [36]. Since the electrical conductivity of manganese oxides is typically low; it shows a relatively low specific capacitance in comparison to its theoretical capacitance value. Creating a ternary composite system by incorporating another material such as a conducting polymer (e.g. polyaniline, polypyrrole, and PEDOT) can improve the specific capacitance [5]. PEDOT exhibits the highest electrical conductivity among these conducting polymers and also exhibits pseudocapacitance. Therefore, it was chosen for use in our composite fibres [37]. CB/CNT/MnO_2 fibres were dip coated in PEDOT:PSS solutions for 5 s, 30 s, 60 s, and 5 minutes. Characteristic peaks of PEDOT were observed in the Raman spectrum of CB/CNT/MnO_2/PEDOT composite fibres (Figure 4H) with the appearance of a strong Raman band centred at 1425 cm^{-1} due to the symmetric stretching mode of the aromatic C=C band of the thiophene rings in PEDOT. The bands usually observed for antisymmetric Cα-Cα, Cβ-Cβ stretching deformations and Cα-Cα inter-ring stretching vibrations located at 1565, 1361 and 1258 cm^{-1} respectively are obscured in this case by the strong Raman vibrations of the CNTs and CB within the fibre. The peak at 961 cm^{-1} is attributed to the oxyethylene ring deformation of PEDOT [38].

SEM imaging of the original Fibre F compared to one coated in MnO_2 and MnO_2-PEDOT (Figure S5) reveals that the surface morphology roughens upon incorporation of MnO_2, with small particles observed on the outside of the fibres. Following dip-coating with PEDOT:PSS the fibre appears smoother, due to the polymer coating, and the SEM image suggests that an even coating has been achieved.

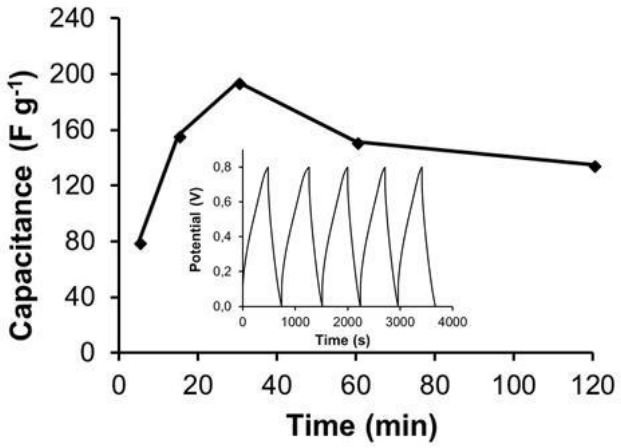
Capacitance (F g-1)
Time (min)
Potential (V)
Time (s)

A

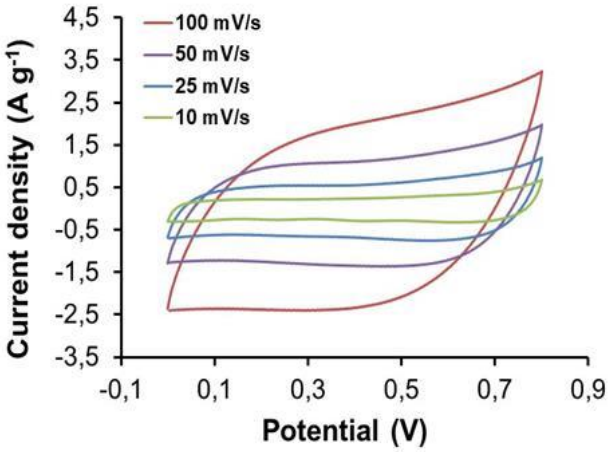
100 mV/s
50 mV/s
25 mV/s
10 mV/s
Current density (A g-1)
Potential (V)

B

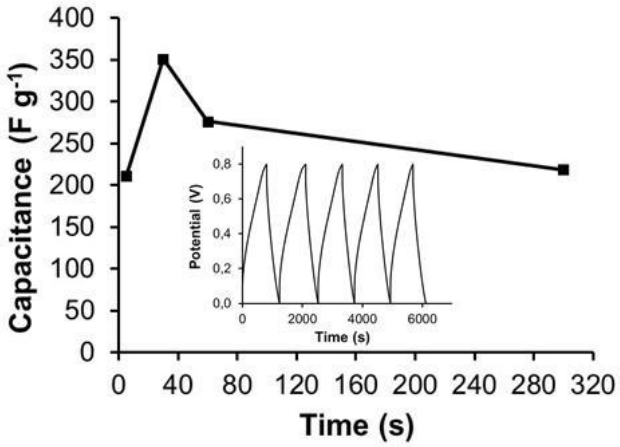
Capacitance (F g-1)
Time (s)
Potential (V)
Time (s)

C

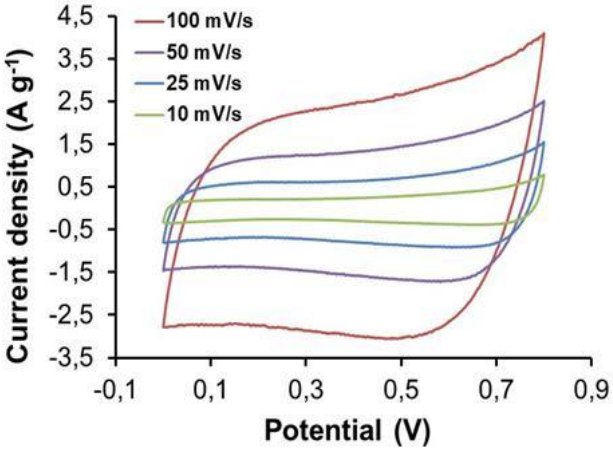
100 mV/s
50 mV/s
25 mV/s
10 mV/s
Current density (A g-1)
Potential (V)

D

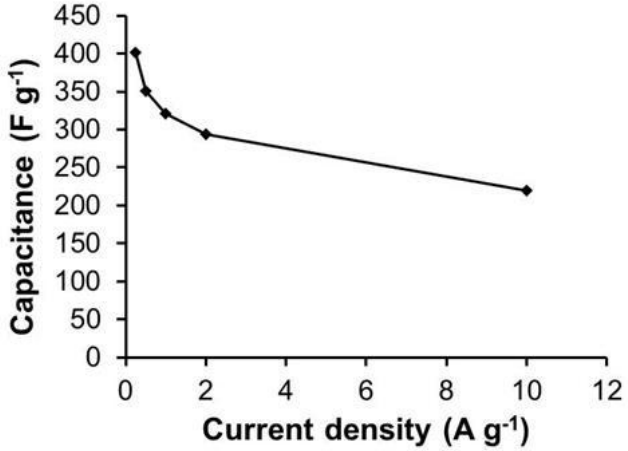
Capacitance (F g-1)
Current density (A g-1)

E

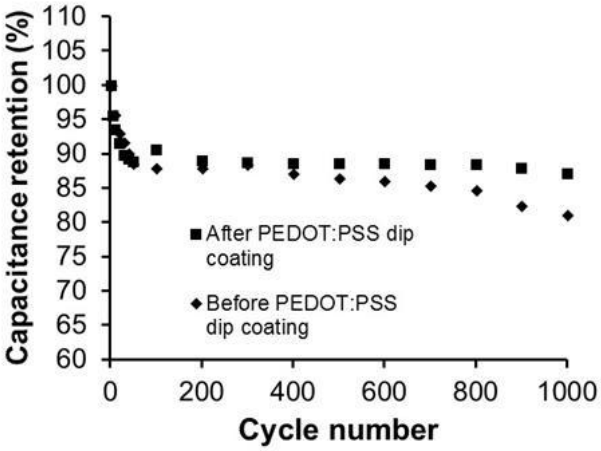
Capacitance retention (%)
After PEDOT:PSS dip coating
Before PEDOT:PSS dip coating
Cycle number

F

Figure 5. (A) Variation of CB/CNT/MnO_2 fibre capacitance with $KMnO_4$ reduction time. Inset shows galvanostatic charge discharge curves for the reduction time of 30 min. Applied intensity: 0.5 A g^{-1}. (B) Cyclic voltammetries from the CB/CNT/MnO_2 fibres (30 min $KMnO_4$ reduction time) at different scan rates. (C) Variation of CB/CNT/MnO_2/PEDOT:PSS fibre capacitance with PEDOT:PSS dip coating time. Inset shows galvanostatic charge discharge curves for fibres dip coated during 30 seconds. Applied intensity: 0.5 A g^{-1}. (D) Cyclic voltammetries from the CB/CNT/MnO_2/PEDOT:PSS fibres (30 min $KMnO_4$ reduction time, 30 seconds PEDOT:PSS dip-coating) at different scan rates. (E) CB/CNT/MnO_2/PEDOT:PSS ternary composite fibres; variation of capacitance with applied intensity. (F) Comparison of cyclic performance for fibres before and after PEDOT:PSS dip coating. Electrolyte: 0.1 mol dm^{-3} KCl Applied intensity: 2 A g^{-1}.

To evaluate the electrochemical properties of the CB/CNT/MnO_2/PEDOT:PSS ternary composite fibre, galvanostatic charge discharge curves were measured for the four different dip-coating times of PEDOT:PSS (Figure 5C). A 30 s dip time yielded the highest specific capacitance for this fibre, 351 F/g, as can be seen in Figure 5D. Differences in the symmetry of the charge discharge curves are observed for the different fibre types (CB/CNT, CB/CNT/MnO_2, CB/CNT/MnO_2/PEDOT:PSS) (Fig. S4, supporting information). In particular, the CB/CNT/MnO_2 and CB/CNT/MnO_2/PEDOT:PSS fibres show an asymmetry between their charge and discharge curves, which is due to the presence of pseudocapacitive materials as previously reported [39-41]. Cyclic voltammetries for the CB/CNT/MnO_2/PEDOT:PSS fibres clearly shows more rectangular-shaped curves and higher current values for the 5-100 mV s^{-1} scan rate range than CB/CNT/MnO_2 fibres, confirming the better energy storage capacity of the former fibres. Moreover, it is seen that the current

response shows the corresponding increases with the increase in the scan rate, indicating a good capacitive behaviour of the CB/CNT/MnO_2/PEDOT:PSS fibres. Thus, the synergistic effect of the different components of the composite electrodes is confirmed: the electrically conducting nature of the CB/CNT fibre and the swelling of the chitosan polymer favours the electrochemical utilization of the MnO_2 and the conducting wrapping layer of PEDOT:PSS further boosts the electrical conductivity and contributes to the pseudocapacitance of the composite electrode. Therefore, a new strategy (wet-spinning of composite materials and solution-based post spinning processes) for electrode design have been tested in order to enhance the capacitance by: (i) increasing electrical conductivity, (ii) facilitating the full utilization of MnO_2 by incorporating carbon nanomaterials and conducting polymers as effective electron pathways, (iii) using different aspect ratio nanomaterials to have more open structures and (iv) using water-swelling polymers like chitosan to improve electrolyte access into the fibre composite. Galvanostatic charge-discharge experiments were further performed at various current densities (Figure 5E). Even when the current density increased by a factor of 20, around 55% of the initial capacitance was retained, indicating a good rate capability of the fibres.

Cycling performance is another key factor for practical applications. Figure 5F compares the performance of the CB/CNT/MnO_2 and CB/CNT/MnO_2/PEDOT:PSS fibres over 1,000 charge-discharge cycles, with the fibres exhibiting retention values of 80.2 ± 0.8 % and 85.1 ± 1.9 % respectively. Improved capacitance retention and fibre stability during cycling is observed with the PEDOT coating, in addition to an overall improved capacitance. The efficiency in our study is similar to those published for fibre electrodes obtained under more complex procedures.

3.5 Solid-state supercapacitor

The CB/CNT/MnO_2/PEDOT composite fibre was assembled into a flexible solid-state supercapacitor device (Figure 6A). Two parallel fibres were coated with PVA-H_3PO_4 gel electrolyte, which acts as both an electrolyte and an effective separator to prevent short circuiting the electrodes. The CV curves of the supercapacitor, both in a straight and bent position (Figure 6B) are symmetrical even at 100 mV s^{-1} indicating good reversibility. Almost identical CV curves are observed for the solid-state device that undergoes cyclic voltammetry while bent.

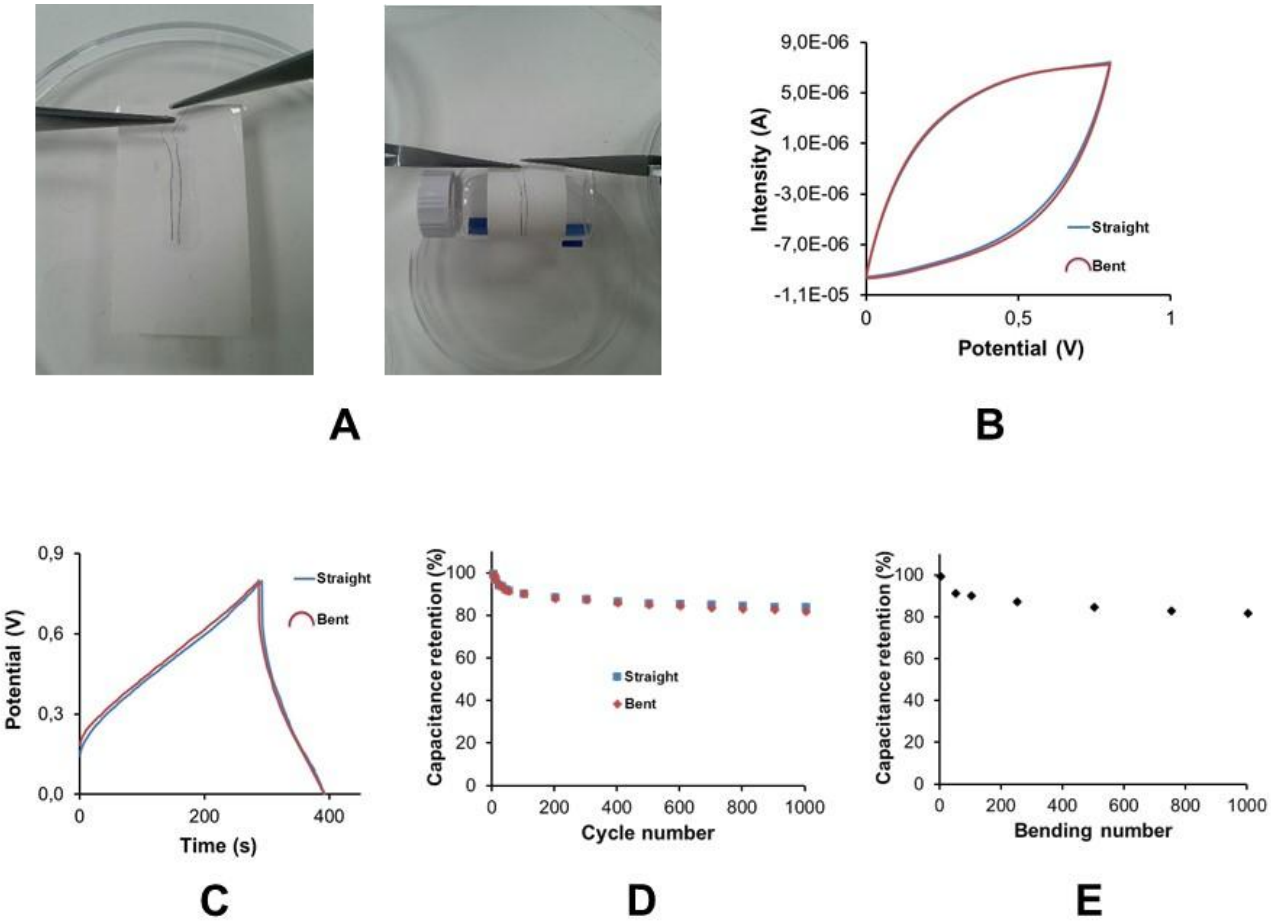

Figure 6. (A) Pictures of the solid state device in straight and bent positions, (B) Cyclic voltammetry, (C) Galvanostatic charge-discharge curves (applied intensity: 2 A g^{-1}), (D)

Cyclic performance over 1000 cycles of the solid state supercapacitor while straight and bent. (E) Bending cycling performance of the fibre device.

Galvanostatic charge-discharge curves (Figure 6C) show a triangular shape, indicating good charge transport between the two electrodes and also indicate that the solid state supercapacitor shows negligible capacitance change on bending. An asymmetric GCD curve for the solid state supercapacitor is observed (Figure 6C), the asymmetry being higher than those previously shown for the single fibres. Comparing the GCD curve of the solid state device with that of the CB/CNT/MnO_2/PEDOT:PSS fibre in aqueous electrolyte, the latter is more symmetric. Factors contributing to such asymmetry include: (i) the presence of pseudocapacitive materials (ii) organic electrolytes have lower electroconductivities than liquid ones and (iii) gel electrolytes have lower electroconductivities than liquid electrolytes [39-41]. The IR drop for the device is also higher than that observed for the fibres in liquid electrolyte, which can be attributed to the internal resistance caused by the gel electrolyte, since the ions move more slowly in the gel than in a liquid. Some alternatives are improving the ionic mobility of the ions in the gel or encapsulating the fibres in a liquid electrolyte.

Despite the IR drop, the specific capacitance value of this solid state device was measured as 51.3 F g^{-1} with good capacitance retentions of 84.2% in straight or 82.3% in bent positions after 1000 charge-discharge cycles (Figure 6D), which suggests no significant differences in the capacitance of the supercapacitor in straight or bent positions. The cyclic performance in this study is comparable with results in similar studies [6,19]. Finally, the capacitance stability of the supercapacitor was evaluated after undergoing 1000 straight-bending cycles. Galvanostatic charge-discharge cycles were recorded after bending the supercapacitor for 50, 100, 250, 500, 750 and 1000 times (Figure 6E). No significant change in the capacitance is

observed after 1000 bending cycles (capacitance retention of 82.1%), suggesting a good electrochemical stability of the supercapacitor after repeated mechanical deformation making it interesting for wearable applications.

Considering the one-dimensional configuration of the electrodes, the longitudinal capacitance of this device is 338 μF cm^{-1} which is greater than twice as high as a fibre supercapacitor based on graphene coated with MnO_2, showing the benefit of the conducting PEDOT coating [42]. These flexible solid-state supercapacitor devices have competitive specific capacitance values and are made *via* simple solution-based processes. This allows fibre-based capacitors to be fabricated in a straightforward continuous process, which is amenable to scale-up, without the need for separate electrochemical deposition steps, or complex multi-step moulding procedures.

4. CONCLUSION

In summary we have successfully fabricated fibre-based supercapacitors by wet-spinning combined with simple solution-based processes that can be included in the wet-spinning procedure. Fibres were initially wet-spun from CNT-carbon black dispersions, followed by chemical reduction to give MnO_2 and finally dip-coating with PEDOT:PSS. These ternary composite fibre electrodes exhibit a high capacitance (351 F g^{-1}) benefitting from the synergistic effect of the pseudocapacitance of the metal oxide and the electrical conductivity of the conducting polymer. A symmetric solid-state device assembled from two composite electrodes shows a specific capacitance of 51.3 F g^{-1}, good long term cyclability (84.2 % capacitance retention after 1000 cycles) and deformation cycling stability (82.1% capacitance retention after 1000 bending cycles).

ACKNOWLEDGEMENTS

The authors acknowledge EPSRC grant number EP/K035002/1.

DATA AVAILABILITY

The raw/processed data required to reproduce these findings cannot be shared at this time due to legal or ethical reasons.

REFERENCES

[1] W. Weng, P. Chen, S. He, X. Sun and H. Peng, Angew. Chem. Int. Ed. 55 (2016) 6140-6169

[2] J. Garcia-Torres, C. Crean and E. Valles, Mater. Design 141 (2018) 9-16

[3] W. Zeng, L. Shu, Q. Li, S. Chen, F. Wang and X.-M. Tao, Adv. Mater. 26 (2014) 5310–5336

[4] X. Yu, Y. Fu, X. Cai, H. Kafafy, H. Wu, M. Peng, S. Hou, Z. Ly, S. Ye and D. Zou, Nano Energy 2 (2013) 1242-1248

[5] S.T. Senthilkumar, Y. Wang and H. Huang, J. Mater. Chem. A 3 (2015) 20863-20879

[6] D. Yu, Q. Qian, L. Wei, W. Jiang, K. Goh, J. Wei, J. Zhang and Y. Chen. Chem Soc. Rev. 44, 2015, 647-662

[7] D.P. Dubal, N.R. Chodankar, D.-H. Kim and P. Gomez-Romero, Chem. Soc. Rev. 47 (2018) 2065-2129

[8] F. Meng, Q. Li, L. Zheng, Energy Storage Materials 8 (2017) 85–109

[9] L. Dai, D.W. Chang, J.B. Baek, W. Lu, Small 8 (2012) 1130-1166

[10] J. Ren, W. Bai, G. Guan, Y. Zhang and H. Peng, Adv. Mater. 25 (2013) 5965-5970

[11] L. Kou, T. Huang, B. Zheng, Y. Han, X. Zhao, K. Gopalsamy, H. Sun and G. Gao, Nat. Commun. 5 (2014) 3754-3763

[12] J. Foroughi, G.M. Spinks, D. Antiohos, A. Mirabedini, A. Gambhir, G.G. Wallace, S.R. Ghorbani, G. Peleckis, M.E. Kozlov, M.D. Lima and R.H. Baughman, Adv. Funct. Mater. 24 (2014) 5859-5865

[13] Z. Cai, L. Li, J. Ren, L. Qiu, H. Lin and H. Peng, J. Mater. Chem. A 1 (2013) 258-261

[14] C. Choi, J.A. Lee, A.Y. Choi, Y.T. Kim, X. Lepró, M.D. Lima, R.H. Baughman and S.J. Kim, Adv. Mater. 26 (2014) 2059–2065

[15] Y. Shang, C. Wang, X. He, J. Li, Q. Peng, E. Shi, R. Wang, S. Du, A. Cao and Y. Li, Nano Energy 12 (2015) 401–409

[16] C. Choi, K.M. Kim, K.J. Kim, X. Lepro, G.M. Spinks, R.H. Baughman and S.J. Kim, Nat. Commun. 7 (2016) 13811-13818

[17] L. Gao, J.A. Surjadi, K. Cao, H. Zhang, P. Li, S. Xu, C. Jiang, J. Song, D. Sun, Y. Lu, ACS Appl. Mater. Interf. 9 (2017) 5409-5418

[18] H.-J. Chu, C.-Y. Lee and N.-H. Tai, RSC Adv. 6 (2016) 111465-111471

[19] G. Qu, J. Cheng, X. Li, D. Yuan, P. Chen, X. Chen, B. Wang and H. Peng, Adv. Mater. 28 (2016) 3646-3652

[20] Z. Xu and C. Gao, Acc. Chem. Res. 47(4) (2014) 1267-1276

[21] C. Lynam, S.E. Moulton and G.G. Wallace, Adv. Mater. 19(9) (2007) 1244-1248

[22] L. Qiu, X. Yang, X. Gou, W. Yang, Z.F. Ma, G.G. Wallace and D. Li, Chemistry–A European Journal 16(35) (2010) 10653-10658

[23] G. Wang, L. Zhang and J. Zhang, Chem. Soc. Rev. 41 (2012) 797–828

[24] M. Toupin, T. Brousse and D. Belanger, Chem. Mater. 16(16) (2004) 3184-3190

[25] H. Adelkham, M. Ghaemi and S.M. Jafari, J. Mater. Sci. Technol. 24(6) (2008) 857-862

[26] L. Yang, S. Cheng, X. Ji, Y. Jiang, J. Zhou and M. Liu, J. Mater. Chem. C 3 (2015) 7338-7344

[27] P. Yang, Y. Ding, Z. Lin, Z. Chen, Y. Li, P. Qiang, M. Ebrahimi, W. Mai, C. P. Wong and Z. L. Wang, Nano Lett. 14 (2014) 731-736

[28] S. Devaraj and N. Munichandraiah, J. Phys. Chem. C 112(11) (2008) 4406-4417

[29] M.S. Dresselhaus, G. Dresselhaus, R. Saito and A. Jorio, Phys. Rep. 409 (2005) 47–99

[30] R. Baddour-Hadjean and J.-P Pereira-Ramos, Chem. Rev. 110 (2010) 1278-1319

[31] C.M. Julien, M. Massot and C. Poinsignon, Spectrochimica Acta Part A 60 (2004) 689–700

[32] G. Han, Y. Liu, L. Zhang, E. Kan, S. Zhang, J. Tang and W. Tang, Sci. Rep. 4 (2014) 4824-4830

[33] Z. Zhang, W. Dang, C. Dong, G. Chen, Y. Wang and H. Guan, RSC Adv. 6 (2016) 6 90002

[34] S.W. Lee, J. Kim, S. Chen, P.T. Hammond and Y. Shao-Horn, ACS Nano 4 (2010) 3889-3896

[35] J-G Wang, F. Kang and B. Wei, Progr. Mater. Sci. 74 (2015) 51-124

[36] S.-B. Yoon and K.-B. Kim, Electrochim. Acta 106 (2013) 135– 142

[37] K. Lakshmi, H. John, R. Joseph, K.E. George and K.T. Mathew, Microwave Opt. Technol. Lett. 50(2) (2008) 504–508

[38] M.C.G. Saborío, S. Lanzalaco, G. Fabregat, J. Puiggalí, F. Estrany and C. Alemán, J. Phys. Chem. C, 122 (2018) 1078-1090

[39] X. Li and B. Wei, Nano Energy 1 **(**2012) 479-487

[40] H. Huang, W. Zhang, Y. Fu and X. Wang, Electrochim. Acta 152 **(**2015) 480-488

[41] T. Xu, X. Ding, Y. Liang, Y. Zhao, N. Chen and L. Qu, Nanoscale 8 (2016) 12133-12117

[42] Q. Chen, Y. Meng, C. Hu, Y. Zhao, H. Shao, N. Chen and L. Qu, J. Power Sources 247 (2014) 32-39